

# The three dynamical fates of Boson Stars

F. S. Guzmán

*Instituto de Física y Matemáticas, Universidad Michoacana de San Nicolás de Hidalgo. Edificio C-3, Cd. Universitaria, 58040 Morelia, Michoacán, México.*

In this manuscript the three types of late-time behavior of spherically symmetric Boson Stars are presented, these are: stable configurations, unstable bounded that collapse to form black holes and unstable unbounded that explode. The results are found by solving the spherically symmetric Einstein-Klein-Gordon system of equations for a complex scalar field with initial conditions corresponding to a Boson Star. The solution is based on a constrained evolution that uses the method of lines for the scalar field and solves the constraint equations for the geometry on the fly.

PACS numbers: 05.30.Jp Boson systems – 04.25.Dm Numerical Relativity – 04.40.-b Self-gravitating systems

## I. INTRODUCTION

Boson stars (BSs) are self-gravitating systems that help illustrating how more complicated systems -like neutron stars- evolve. Nevertheless, BSs have been studied not only as toy models but have also been considered as potentially existing astrophysical objects. In this sense, BSs can be assumed to exist because they can be considered to represent the final stage of zero temperature self-gravitating Bose Condensates [1], with regular geometry and smooth matter distribution, with no horizons or singularities. Because these objects do not emit in the electromagnetic spectrum and do not interact in any way except through gravity, they are transparent. In fact BSs are studied as potential black hole candidates, with results that discard their existence like those presented in [2], others showing that there must be significant differences when the model considers an accretion disk [3], and a third position showing that by choosing the correct boson star, such star can mimic the behavior of a black hole [21]. In a different context, the Newtonian version of BSs has been considered as model of galactic halos explaining the galaxy formation process under the scalar field dark matter hypothesis [1, 5–7]. For reviews on BSs see [8, 9].

The association of BSs with astrophysical objects may become important when possible astrophysical measurable signals related to these objects might be at hand soon. This is the case of gravitational wave (GW) astronomy. There are already some results related to the GW signals sourced by boson stars, either single stars perturbed with shells of particles [10] or binary boson star systems [11]. The key point is that as gravitational wave sources are analyzed numerically, the technology is also applicable to the study of BS systems.

BS solutions, as happens with other type of general relativistic self-gravitating configurations, define stable and unstable branches. Nevertheless, the BS unstable branch shows a rather strange property, that is, there are unstable configurations that collapse into black holes and others that disperse away, because the binding energy is allowed to be negative or positive. It calls the attention that the later configurations have not been studied sufficiently, and here we present important properties

of this type of configurations. The results presented in this paper confirm and illustrate, in the full non-linear regime, the three behaviors using the integration of an initial value problem using numerical in spherical symmetry. This study was presented before for the bounded cases [12, 13]. An unbounded case was presented in [14] in full 3D numerical simulations and confirmed here with a different set up, which supports the predictions from perturbation theory (see e.g. [15, 16]).

The paper is organized as follows: in Section II the usual algorithm to construct BS configurations is shown, in Section III the algorithm used here to evolve BSs is presented; in Section IV the configurations for the different types of behavior are selected; in Section V basic tests are shown for stable configurations; in Section VI and VII the expected behavior of unstable bounded and unbounded configurations (respectively) is presented; finally in Section VIII a few comments are mentioned.

## II. BOSON STAR CONFIGURATIONS

BSs arise from the Lagrangian density of a complex scalar field minimally coupled to gravity, that is:

$$\mathcal{L} = -\frac{R}{\kappa_0} + g^{\mu\nu} \partial_\mu \phi^* \partial_\nu \phi + V(|\phi|^2), \quad (1)$$

where  $\kappa_0 = 16\pi G$  in units where  $c = \hbar = 1$ ,  $\phi$  is the scalar field, the star stands for complex conjugate and  $V$  is the potential of the field [8, 9]. Notice that this Lagrangian density is invariant under the global  $U(1)$  group, and the associated conserved charge is the amount called number of particles (defined below). When the action is varied with respect to the metric Einstein's equations arise  $G_{\mu\nu} = \kappa_0 T_{\mu\nu}$ , with the following stress-energy tensor

$$T_{\mu\nu} = \frac{1}{2}[\partial_\mu \phi^* \partial_\nu \phi + \partial_\mu \phi \partial_\nu \phi^*] - \frac{1}{2}g_{\mu\nu}[\phi^{*\alpha} \phi_{,\alpha} + V(|\phi|^2)]. \quad (2)$$

Boson stars are related to the potential  $V = m^2|\phi|^2 + \frac{\lambda}{2}|\phi|^4$ , although the name Boson Star has been applied to solutions using other types of potentials (see e.g. [17]).

The quantity  $m$  is understood as the mass of the boson and  $\lambda$  is the coefficient of a two body self-interaction mean field approximation. The Bianchi identity reduces to the Klein-Gordon equation

$$\left(\square - \frac{dV}{d|\phi|^2}\right)\phi = 0, \quad (3)$$

where  $\square\phi = \frac{1}{\sqrt{-g}}\partial_\mu[\sqrt{-g}g^{\mu\nu}\partial_\nu\phi]$ .

Boson stars (BSs) are spherically symmetric solutions to the above set of equations under a particular condition: the scalar field has a harmonic time dependence  $\phi(r, t) = \phi_0(r)e^{-i\omega t}$ , where  $r$  is the radial spherical coordinate. This condition implies that the stress energy tensor in (2) is time-independent, which implies through Einstein's equations that the geometry is also time-independent. That is, there is a time-dependent scalar field oscillating upon a time-independent geometry whose source is the scalar field itself. It is possible to construct solutions for boson stars assuming that the metric can be written in normal coordinates as

$$ds^2 = -\alpha(r)^2 dt^2 + a(r)^2 dr^2 + r^2 d\Omega^2. \quad (4)$$

For these coordinates the Einstein-Klein-Gordon (EKG) system of equations reads:

$$\begin{aligned} \frac{\partial_r a}{a} &= \frac{1-a^2}{2r} + \\ &\quad \frac{1}{4}\kappa_0 r \left[ \omega^2 \phi_0^2 \frac{a^2}{\alpha^2} + (\partial_r \phi_0)^2 + a^2 \phi_0^2 (m^2 + \frac{1}{2}\lambda \phi_0^2) \right], \\ \frac{\partial_r \alpha}{\alpha} &= \frac{a^2-1}{r} + \frac{\partial_r a}{a} - \frac{1}{2}\kappa_0 r a^2 \phi_0^2 (m^2 + \frac{1}{2}\lambda \phi_0^2), \\ \partial_{rrr} \phi_0 + \partial_r \phi_0 \left( \frac{2}{r} + \frac{\partial_r \alpha}{\alpha} - \frac{\partial_r a}{a} \right) + \omega^2 \phi_0 \frac{a^2}{\alpha^2} \\ &\quad - a^2 (m^2 + \lambda \phi_0^2) \phi_0 = 0. \end{aligned} \quad (5)$$

This system is a set of coupled ordinary differential equations to be solved under the conditions of spatial flatness at the origin  $a(0) = 1$ ,  $\phi_0(0)$  finite and  $\partial_r \phi_0(0) = 0$  in order to guarantee regularity and spatial flatness at the origin, and  $\phi_0(\infty) = \phi_0'(\infty) = 0$  in order to ensure asymptotic flatness at infinity as described in [12, 13, 15, 18, 19]; these conditions reduce the system (5) to an eigenvalue problem for  $\omega$ , that is, for every central value of  $\phi_0$  there is a unique  $\omega$  with which the boundary conditions are satisfied. Equations (5) have several coefficients that can be removed with a rescaling. In order to do so, the following transformation works:  $\tilde{\phi}_0 = \sqrt{\frac{\kappa_0}{2}}\phi_0$ ,  $\tilde{r} = mr$ ,  $\tilde{t} = \omega t$ ,  $\tilde{\alpha} = \frac{m}{\omega}\alpha$  and  $\tilde{\Lambda} = \frac{2\lambda}{\kappa_0 m^2}$ . The result is that the physical constants vanish from the equations, the radial coordinate has units of  $m$  and time has units of  $\omega$ . After substituting this transformation and removing the tildes from everywhere, the resulting EKG system of equations reads:

$$\begin{aligned} \frac{\partial_r a}{a} &= \frac{1-a^2}{2r} + \\ &\quad \frac{1}{2}r \left[ \phi_0^2 \frac{a^2}{\alpha^2} + (\partial_r \phi_0)^2 + a^2 (\phi_0^2 + \frac{1}{2}\Lambda \phi_0^4) \right], \\ \frac{\partial_r \alpha}{\alpha} &= \frac{a^2-1}{r} + \frac{\partial_r a}{a} - r a^2 \phi_0^2 (1 + \frac{1}{2}\Lambda \phi_0^2), \\ \partial_{rrr} \phi_0 + \partial_r \phi_0 \left( \frac{2}{r} + \frac{\partial_r \alpha}{\alpha} - \frac{\partial_r a}{a} \right) + \phi_0 \frac{a^2}{\alpha^2} \\ &\quad - a^2 (1 + \Lambda \phi_0^2) \phi_0 = 0. \end{aligned} \quad (6)$$

These equations are solved using finite differences with an ordinary integrator (adaptive step-size fourth order Runge-Kutta algorithm in the present case) and a shooting routine that bisects the value of  $\omega$ .

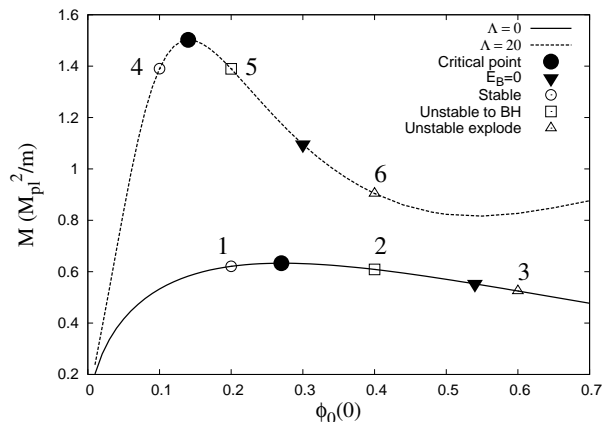


FIG. 1: Sequences of equilibrium configurations for two values of  $\Lambda$  are shown as a function of the central value of the scalar field  $\phi_0(0)$ ; each point of the curves corresponds to a solution of the eigenvalue problem and represents a boson star configuration. The filled circles indicate the critical solution that separates the stable from the unstable branch. Those configurations to the left of the maxima represent stable configurations. The inverted triangles indicate the point at which the binding energy is zero. Those configurations between the filled circles and the inverted triangles (along each sequence) collapse into black holes as a response to a perturbation. Configurations to the right of the inverted triangles disperse away.

The solutions of (6) define sequences of equilibrium configurations like those shown in Fig. 1. Each point in the curves corresponds to a boson star solution. In each of the curves two important points for each value of  $\Lambda$  are marked: i) the critical point -marked with a filled circle- indicating the threshold between the stable and unstable branches of each sequence, that is, configurations to the left of this point are stable and those to the right are unstable as found through the analysis of perturbations [15, 19], catastrophe theory [16] and full non-linear evolution of the equilibrium solutions [12–14] and ii) the point at which the binding energy  $E_B = M - Nm = 0$  marked with an inverted filled triangle (see [15] for this convention of the binding energy),

where  $N = \int j^0 d^3x = \int \frac{i}{2} \sqrt{-g} g^{\mu\nu} [\phi^* \partial_\nu \phi - \phi \partial_\nu \phi^*] d^3x$  is the number of particles; that is, the conserved quantity due to the invariance under the global  $U(1)$  group of the Lagrangian density (1).  $M = (1 - 1/a^2)r/2$  evaluated at the outermost point of the numerical domain is the Misner-Sharp mass; the configurations between the instability threshold and the zero binding energy point have negative binding energy ( $E_B < 0$ ) and collapse into black holes whereas those to the right have positive binding energy and are expected to disperse away. Stable configurations, obviously have negative binding energy. The non-filled circles, triangles and squares pointed out in the plot correspond to the six configurations chosen as special cases to be explored here.

### III. THE EVOLUTION OF BOSON STARS

In order to verify the fate of Boson Stars one has to evolve them. For this it is necessary to relax the condition of stationarity of space-time and allow the scalar field and space-time metric to evolve. Then Boson Star configurations constructed so far, both scalar field profile and metric functions, will work only as initial conditions for an initial value problem associated to the EKG equations.

For the construction of the evolution equations we split the scalar field into its real and imaginary parts  $\phi = \phi_1 + i\phi_2$ . In this way, the Klein Gordon equation becomes two equations:

$$\left(\square - \frac{dV}{d|\phi|^2}\right)\phi_1 = 0, \quad \left(\square - \frac{dV}{d|\phi|^2}\right)\phi_2 = 0. \quad (7)$$

Another major point is that as time-dependence of the space-time is going to be allowed, the space-time metric has to be relaxed to:

$$ds^2 = -\alpha(r, t)^2 dt^2 + a(r, t)^2 dr^2 + r^2 d\Omega^2, \quad (8)$$

where time dependence of  $\alpha$  and  $a$  has been allowed, but the gauge is such that the radial coordinate has been kept the same. Using this new line element for the space-time, it is convenient to define first order variables for the scalar field:  $\pi_i = \frac{a}{\alpha} \partial_t \phi_i$  and  $\psi_i = \partial_r \phi_i$ , for each  $i = 1, 2$ . With these new variables and metric (8) the KG equations are translated into the following set of first order PDEs

$$\begin{aligned} \partial_t \phi_1 &= \frac{\alpha}{a} \pi_1, \\ \partial_t \phi_2 &= \frac{\alpha}{a} \pi_2, \\ \partial_t \psi_1 &= \partial_r \left( \frac{\alpha}{a} \pi_1 \right), \\ \partial_t \psi_2 &= \partial_r \left( \frac{\alpha}{a} \pi_2 \right), \\ \partial_t \pi_1 &= \frac{1}{r^2} \partial_r \left( r^2 \frac{\alpha}{a} \psi_1 \right) - a\alpha \frac{dV}{d|\phi|^2} \phi_1, \\ \partial_t \pi_2 &= \frac{1}{r^2} \partial_r \left( r^2 \frac{\alpha}{a} \psi_2 \right) - a\alpha \frac{dV}{d|\phi|^2} \phi_2. \end{aligned} \quad (9)$$

On the other hands, in terms of the first order variables and the line element (8), Einstein's equations read:

$$\frac{\partial_r a}{a} = \frac{1 - a^2}{2r} + \frac{r}{2} [\pi_1^2 + \pi_2^2 + \psi_1^2 + \psi_2^2 + a^2 V], \quad (10)$$

$$\frac{\partial_r \alpha}{\alpha} = \frac{a^2 - 1}{r} + \frac{a'}{a} - r a^2 V, \quad (11)$$

$$\partial_t a = \alpha r [\psi_1 \pi_1 + \psi_2 \pi_2]. \quad (12)$$

These equations correspond to the Hamiltonian constraint, the slicing condition and the momentum constraint. Clearly, this set of three equations is overdetermined, and it is necessary to choose two of these three equations as the set to be solved.

The system of equations to be solved is (9) together with (12), which constitutes a constrained evolution system. Among the Einstein's equations we choose to solve (10) and (11) and only monitor the validity of (12) during the evolution.

The solution is as follows. Equations (9) are solved using the method of lines with second order accurate stencils and a third order Runge-Kutta time integrator. Constraint equations (10) and (11) are solved using a fourth order Runge-Kutta ODE solver at all intermediate steps required during the integration of (9).

The boundary condition for the scalar field is that of an outgoing spherical wave on a Schwarzschild background, which in its differential equation form reads:

$$\partial_r \pi_i + \partial_t \pi_i + \pi_i / r = 0, \quad \psi_i = -\pi_i - \phi_i / r, \quad (13)$$

for each  $i = 1, 2$ . That is, the real and imaginary parts of the scalar field are considered to behave as outgoing spherical waves separately. This is a quite simple boundary condition that certainly can be improved, the only requirement demanded in the present analysis is that the boundary conditions allow second order convergence after various crossing times. These conditions were implemented using a second order accurate upwind stencils.

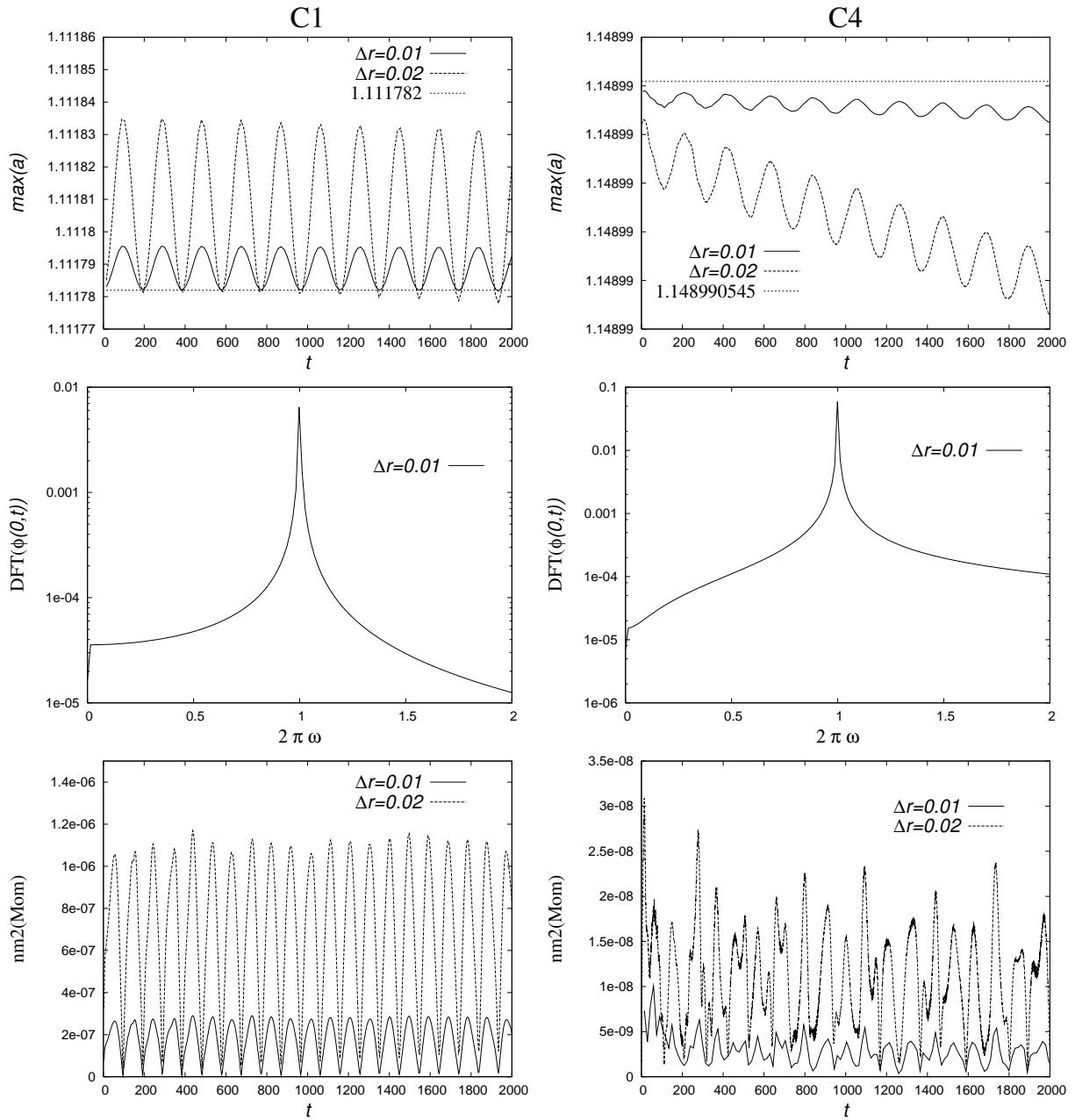


FIG. 2: (top) Convergence of  $a_{max}$  for configurations 1 and 4. The constant line indicates the value of  $a_{max}$  at initial time, which is assumed to be the value it should keep during the evolution. Second order convergence to such value during the evolution is a good indicator that the evolution is being carried out properly. (Middle) Fourier Transform of the central value of the field for the same configurations. The peak shows up at  $\omega = \frac{1}{2\pi}$ . This test indicates that the scalar field is oscillating with the correct frequency. (Bottom) Convergence of the  $L_2$  norm of the momentum constraint; the aim of these plots is to show that the momentum constraint is satisfied in the continuum limit. The numerical parameters are as indicated in the plots: two resolutions were used for the convergence test.

#### IV. PREPARING THE STATES

In order to illustrate the three types of fate for Boson stars, we choose three configurations for each of the two values of the self-interaction  $\Lambda = 0, 20$ , that clearly indicate the expected behavior. According to the labels in Fig. 1, the theory predicts that configurations 1 and 4

should remain stable, configurations 2 and 5 should collapse to black holes and configurations 3 and 6 should disperse away.

In Table I we summarize the properties of the configurations chosen. The selected stable configurations were not perturbed so that it was possible to track the convergence toward a time-independence geometry, whereas we

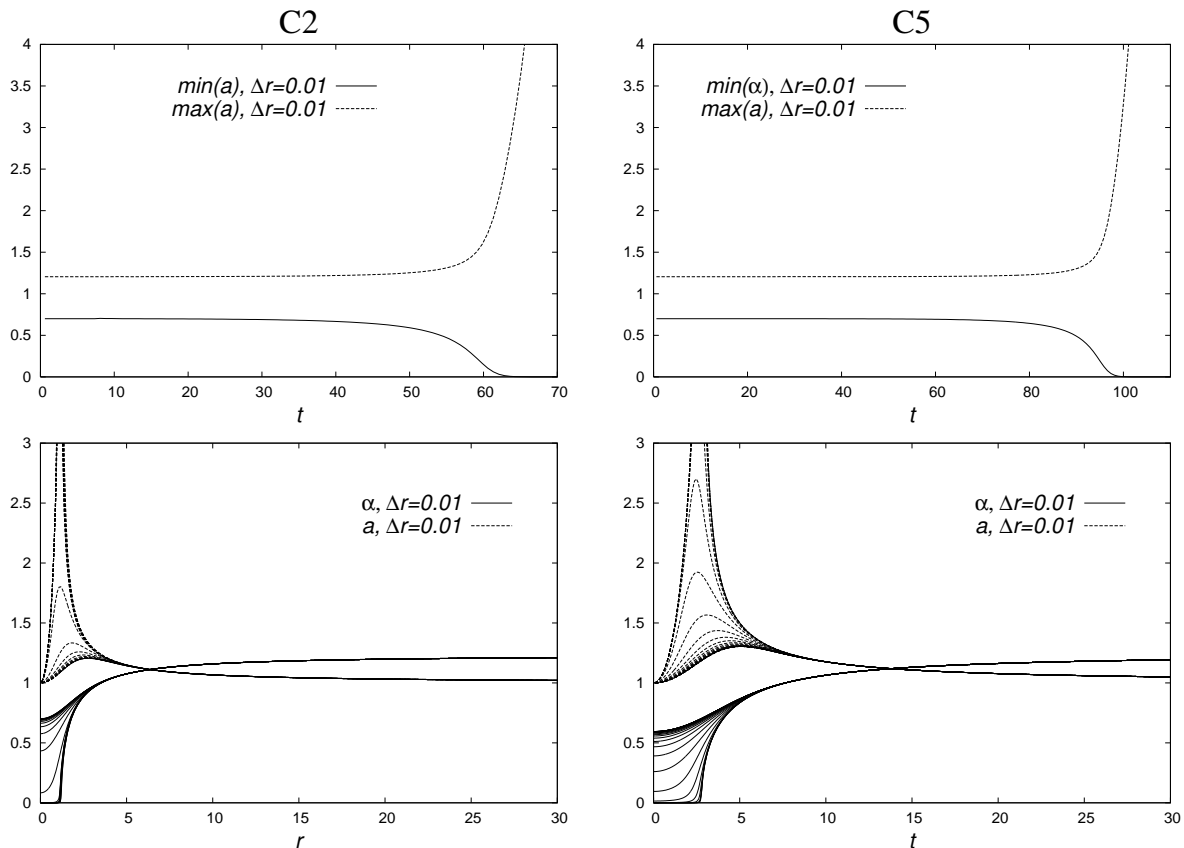


FIG. 3: (Top) Maximum of the metric function  $a$  and minimum of  $\alpha$ . What is shown is the collapse of the lapse and the divergence of  $a$ , indicating the formation of a horizon in the coordinates that are being used. (Bottom) Snapshots of  $a$  and  $\alpha$  that show the process of collapse. The resolution used is the one shown in the plots.

Label	$M$	$M_{pert}$	%	$r_{95}$	$r_0$	$A$
C1	0.620882		0.	7.66		
C2	0.608758	0.60937	0.1	4.84	6.	0.0008
C3	0.5248	0.52537	0.1086	3.68	5.	0.0012
C4	1.390156		0.	12.27		
C5	1.389544	1.39101	0.105	7.62	9.	0.0008
C6	0.9043	0.905234	0.103	5.66	7.	0.0008

TABLE I: Configurations used to present the three different types of behavior. The properties of the Gaussian shell acting as perturbation and the magnitude in percent of the perturbation are mentioned. The perturbation profile is  $A \exp(-(r - r_0)^2/0.1)$ .  $M$  is the mass of the unperturbed Boson Star,  $M_{pert}$  is the mass of the perturbed Star, % indicates the percent of mass the perturbation contributes with,  $r_{95}$  is the radius of the Star containing 95 per cent of the total mass of the star.

used a gaussian shell to trigger the instability of unstable configurations.

## V. STABLE CONFIGURATIONS

The test consists in showing the validity of the hypotheses used in the construction of BS solutions (harmonic time dependence of the scalar field and time independence of the metric functions). The configurations proposed for the test are the configurations marked with unfilled circles and numbers 1 and 4 in Fig. 1.

In the top of Fig. 2 the maximum of the metric function  $a$  is shown. Due to the discretization error, the configurations are perturbed permanently, and therefore the metric is oscillating in time. The point is that one has to show the amplitude of the oscillations converges to zero in the continuum limit, which is equivalent to have convergence of  $a_{max}$  to the value it should keep during the evolution, which we consider to be the value of  $a_{max}$  calculated for the equilibrium configuration at initial time. Since the stencils of the finite differences used to solve the evolution system are second order accurate, the departure from the equilibrium configuration should reduce by a factor of four when doubling the resolution, which is exactly what is shown at the top of Fig. 2, because the amplitude of oscillations is four times bigger when using resolution  $\Delta r = 0.02$  than when using  $\Delta r = 0.01$ .

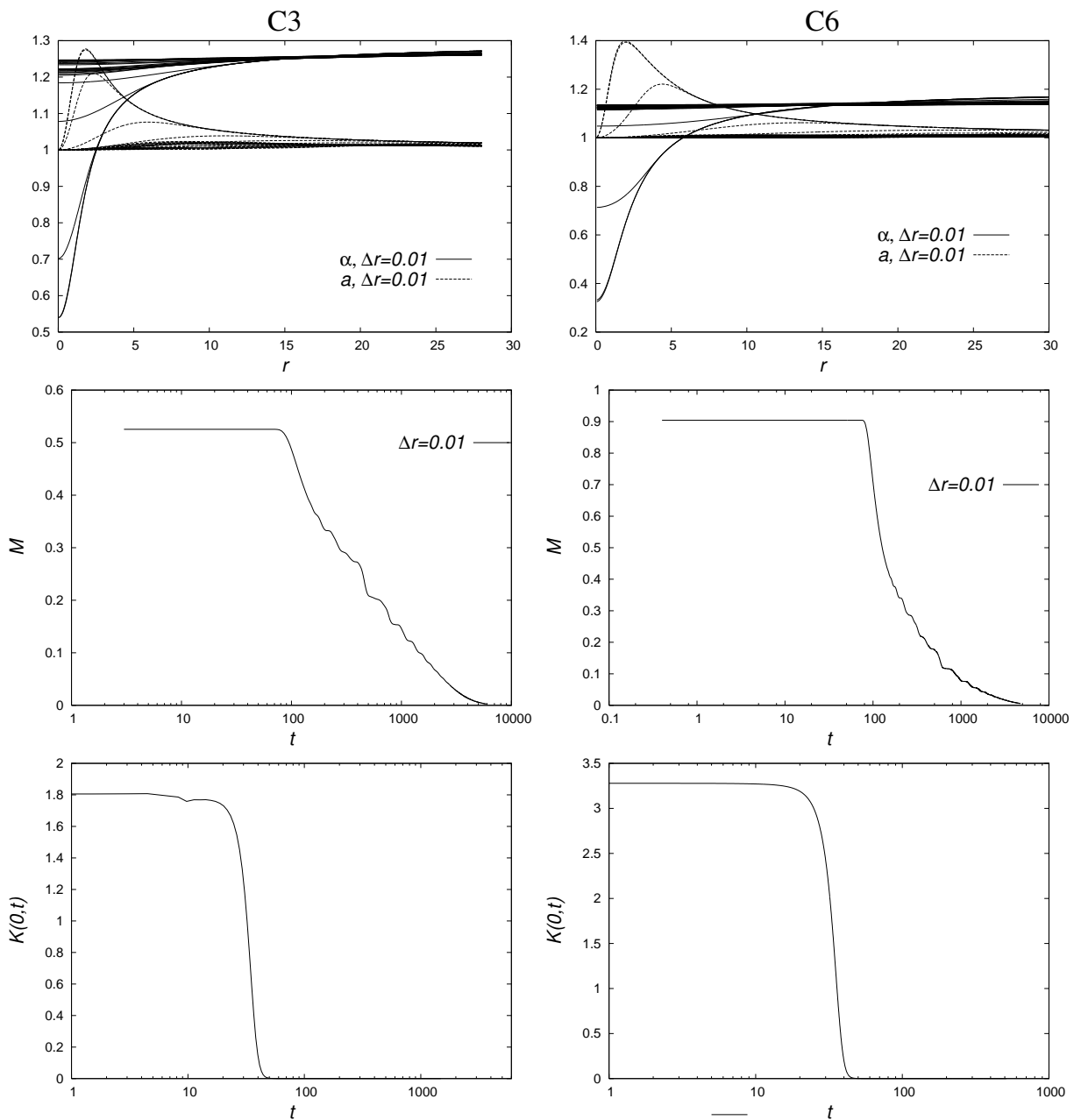


FIG. 4: (Top) Snapshots of the metric functions for configurations C3 and C6, illustrating that the metric evolves toward the flat metric. (Middle) Mass vs time of the system, which shows that the configurations are releasing all its mass toward infinity. (Bottom) Central value of the Kretschmann scalar, which tends to zero with the pass of time. The resolution used is indicated in the plots.

Another test of the correct evolution consists in showing that the scalar field is truly oscillating meanwhile with the correct frequency. In the middle panel of Fig. 2 the Fourier Transform of the central value of  $\phi_1$  is shown. The result indicates that the frequency of oscillation of the scalar field corresponds to the eigenvalue calculated when solving the initial value problem (remember the time was rescaled to be  $\tilde{t} = \omega t$ ). In the units used here, where  $t \rightarrow \omega t$ , the frequency is  $\omega = 1/2\pi$ .

Finally let us discuss the momentum constraint. Since

the stencils of the finite differences used to solve the evolution system are second order accurate, the momentum constraint (12) is not satisfied exactly, instead  $\partial_t a - \alpha r[\psi_1 \pi_1 + \psi_2 \pi_2] = \mathcal{O}(\Delta r^2)$ , therefore the violation of this constraint should reduce quadratically with resolution. For the verification of convergence it suffices to check whether a norm of the violation, which is actually defined at each time step over the spatial domain, converges. In the bottom panel of Fig. 2 we show the  $L_2$  norm of the violation as a function of time, using reso-

lutions  $\Delta r = 0.01, 0.02$  and the fact that the violation using the coarse resolution is four times bigger than with the fine resolution, shows the second order convergence of the violation to zero in the continuum limit.

No explicit perturbations are applied in the stable case. Instead, measuring the correct frequency of oscillation of the scalar field determines whether or not the evolution code is working properly or not. Applying explicit perturbations to the particle number of these stable configurations would imply a more dynamical behavior, and the amplitude decay of the maximum of the metric function  $a$  could be studied as done in [13].

## VI. BOUNDED UNSTABLE CONFIGURATIONS

For this second scenario we choose the adequate configurations 2 and 5, which have a negative binding energy. In principle, the discretization error would provide a strong enough perturbation to collapse the configuration. However, in order to have a quicker collapse we use a small perturbation consisting of the addition of a Gaussian shell to the real part of the scalar field, with properties shown in Table I. Then the equations for  $\alpha$  and  $a$  are resolved before starting the evolution. The amplitude of the Gaussian shell is positive and the number of particles is increased by a small fraction of its initial value.

The results of the evolution are summarized in Fig. 3, where snapshots of the lapse and  $a$  are shown; in fact the lapse collapses to zero in a region expected to be covered by a horizon and the metric function  $a$  starts diverging due to the slice-stretching effect when using normal coordinates [20]. In the coordinates used, an apparent horizon has been formed when the lapse is sufficiently near to zero. However, it is simple to use different coordinates allowing one to calculate the location, mass and possible oscillations of an apparent horizon. The whole process where apparent and event horizons was calculated during the collapse of an unstable BS can be found in [14]. Up to this point the results in this section correspond to the typical results found for spherically symmetric BSs in the canonical papers [12, 13].

## VII. UNBOUNDED UNSTABLE CONFIGURATIONS

In this case, the binding energy is positive, which means that there is no work needed to disassemble the configuration, a case that is barely mentioned in BSs studies. A previous case of fissioned BS was found in [14], in the context of the full 3D unconstrained evolution of BSs in 3+1 Numerical Relativity.

In Fig. 4 the results for configurations 3 and 6 are shown with three different elements: i) the metric function  $a$  and the lapse  $\alpha$  become constant after a while dur-

ing the evolution, ii) the mass function  $M$  decays to zero during the same time-scale, and iii) the central value of the Kretschmann scalar  $K$  becomes zero, in order to have an indication that no singularities are left behind the exploding scalar field. This is supported by the fact that the metric at the origin is spatially flat with a non-zero lapse.

The perturbation consisted in the addition of a tiny fraction of particles again, even though, the configurations reacted in a very explosive way. The property assumed to be the responsible for this explosive behavior is the one argued as the responsible to work against the gravitational collapse of the bosons, that is, the uncertainty principle, as opposed to the degeneracy pressure that prevents the gravitational collapse of fermionic stars. The implication of the uncertainty principle is therefore that the configuration has an excess of kinetic energy to compensate the localization of the wave function.

## VIII. FINAL REMARKS

Among the three types of boson stars presented here, only the stable type has been studied with certain attention, and stable configurations are proposed either as potential existing objects or as toy models. Perhaps unstable configurations might impose restrictions on mass and self-interaction of Boson Stars as models that attempt to supplant black holes [3, 21, 22], or in the low energy and weak field limit, scalar fields playing the role of -for instance- dark matter [1] might also be restricted.

### Appendix A: Kretschmann invariant

We use the central value of the Kretschmann invariant, in order to easily see the formation of a singularity. The expression for the metric (8) is:

$$\begin{aligned}
 K = & -\frac{16\dot{a}^2}{r^2\alpha^2a^4} + \frac{4(\alpha'')^2}{\alpha^2a^4} - \frac{8\alpha''\ddot{a}}{\alpha^3a^3} + \frac{8\alpha''\dot{a}\dot{a}}{\alpha^4a^3} \\
 & - \frac{8\alpha''\alpha'a'}{\alpha^2a^5} + \frac{4(\ddot{a})^2}{\alpha^4a^2} - \frac{8\dot{a}\dot{a}\dot{a}}{\alpha^5a^2} + \frac{8\dot{a}\alpha'a'}{\alpha^3a^4} \\
 & + \frac{4(\dot{\alpha})^2(\dot{a})^2}{\alpha^6a^2} - \frac{8\dot{\alpha}\dot{a}\alpha'a'}{\alpha^4a^4} + \frac{4(\alpha')^2(a')^2}{\alpha^2a^6} + \frac{8(\alpha')^2}{r^2\alpha^2a^4} \\
 & + \frac{8(a')^2}{r^2a^6} + \frac{4}{r^4} - \frac{8}{r^4a^2} + \frac{4}{r^4a^4}.
 \end{aligned}$$

### Acknowledgments

This work is partly supported by projects CIC-UMSNH-4.9, CONACyT 79995 and PROMEP-UMICH-CA-22.

- 
- [1] F. S. Guzmán and L. A. Ureña-López, *ApJ* **645**, 814 (2006). ArXiv: astro-ph/0603613.
- [2] Y-F. Tuan, R. Narayan and M. J. Rees, *ApJ* **606**, 1112 (2004).
- [3] D. F. Torres, *Nucl. Phys.* **B 26**, 377 (2002).
- [4] F. S. Guzmán, *Phys. Rev. D* **73**, 021501 (2006). ArXiv: gr-qc/0512081.
- [5] A. Bernal and F. S. Guzmán, *Phys. Rev. D* **74**, 063504 (2006). ArXiv: astro-ph/0608523.
- [6] A. Bernal and F. S. Guzmán, *Phys. Rev. D* **74**, 103002 (2006). ArXiv: astro-ph/0610682.
- [7] E. W. Mielke and J. A. Vélez-Pérez, *Phys. Rev. D* **75** 043504 (2007). *Ibid*, *Phys.Lett.* **B 671** 174 (2009).
- [8] Ph. Jetzer, *Phys. Rep.* **220** 163, 1992.
- [9] F. E. Schunck, E. W. Mielke, *Class. Quantum Grav.* **20** R301-R356.
- [10] J. Balakrishna, R. Bondarescu, G. Daues, F. S. Guzmán, E. Seidel, *Class. Quantum Grav.* **23**, 2631-2652 (2006). ArXiv: gr-qc/0602078.
- [11] C. Palenzuela, I. Olabarrieta, L. Lehner, S. Liebling, *Phys. Rev. D* **75**, 064005, 2007. ArXiv: gr-qc/0612067.
- [12] E. Seidel and W-M. Suen, *Phys. Rev. D* **42**, 384 (1990).
- [13] J. Balakrishna, E. Seidel and W-M. Suen, *Phys. Rev. D* **58**, 104004 (1998).
- [14] F. S. Guzmán, *Phys. Rev. D* **70**, 044033 (2004).
- [15] M. Gleiser, *Phys. Rev. D* **38**, 2376 (1988).
- [16] F. V. Kusmartsev, et al., *Phys. Rev. D* **43**, 3895 - 3901 (1991).
- [17] F. E. Schunck and D. F. Torres, *Int. J. Mod. Phys. D* **9** (2000) 601.
- [18] R. Ruffini and S. Bonazzolla, *Phys. Rev.* **187**, 1767 (1969).
- [19] S. H. Hawley and M. W. Choptuik, *Phys. Rev. D* **62**, 104024 (2000).
- [20] M. Alcubierre, *Introduction to 3+1 Numerical Relativity*, Oxford University Press, 2008.
- [21] F. S. Guzmán, *Phys. Rev. D* **73** 021501(R) (2006).
- [22] F. S. Guzmán, J. M. Rueda Becerril, *Phys. Rev. D* **80**, 084023 (2009).